Zn:In(OH)$_y$S$_z$ Solid Solution Nanoplates: Synthesis, Characterization, and Photocatalytic Mechanism

LI-SHA ZHANG,[†] KIN-HANG WONG,[†] DIE-QING ZHANG,[‡] CHUN HU,[§] JIMMY C. YU,[‡] CHIU-YEUNG CHAN,[∥] AND PO-KEUNG WONG*[,†,⊥]

Department of Biology, The Chinese University of Hong Kong, Shatin, NT, Hong Kong SAR, China, Department of Chemistry, The Chinese University of Hong Kong, Shatin, NT, Hong Kong SAR, China, State Key Laboratory of Environmental Aquatic Chemistry, Research Center for Eco-Environmental Sciences, Chinese Academy of Sciences, Beijing 100085, China, Department of Microbiology, The Chinese University of Hong Kong, Shatin, N.T., Hong Kong SAR, China, and Environmental Science Programme, The Chinese University of Hong Kong, Shatin, N.T., Hong Kong SAR, China

Received July 12, 2009. Revised manuscript received August 20, 2009. Accepted August 21, 2009.

Zn:In(OH)$_y$S$_z$ solid solution nanoplates (Zn:In(OH)$_y$S$_z$-SSNs) with uniform nanoparticle size were synthesized through a simple sodium dodecyl sulfate (SDS)-assisted hydrothermal process. To achieve better photoabsorption in the visible light (VL) region and suitable redox potentials of the Zn:In(OH)$_y$S$_z$ solid solution (Zn:In(OH)$_y$S$_z$-SS), the substitution of S^{2-} for OH^- was carried out by adjusting the concentration of thiourea and SDS in the synthesis solution, while the doping of Zn^{2+} was realized by adjusting Zn^{2+} concentration. In addition, the morphology and crystallinity of Zn:In(OH)$_y$S$_z$-SSs were also controlled by the concentration of SDS. Using Rhodamine B (RhB) as a target pollutant, the photocatalytic performance of these Zn:In(OH)$_y$S$_z$-SSs with different components, diameter sizes, and morphologies was investigated. Remarkably, Zn:In(OH)$_y$S$_z$-SSNs prepared with atomic ratio of Zn^{2+} and In^{3+} of 0.6, 45 mmol L^{-1} thiourea, and 26 mmol L^{-1} SDS, have the highest visible-light-driven (VLD) photocatalytic activity, exceeding 95% for the degradation of RhB after 60 min. The investigation of photocatalytic mechanism further indicates that the holes, superoxide radical ($\cdot O_2^-$) and surficial hydroxyl radical ($\cdot OH_s$) are the major reactive species for the photocatalytic reactions. More importantly, for the first time, a simple and versatile strategy is developed to confirm the fact that direct contact between the Zn:In(OH)$_y$S$_z$-SS and RhB is the prerequisite for the photocatalytic degradation of RhB. Therefore, we report not only the preparation of a novel and effective VL-driven photocatalyst, but also provide mechanistic insight into semiconductor photocatalysis.

1. Introduction

Photocatalysis is a green and energy-saving technology for the treatment of all kinds of contaminants, especially for the removal of organic contaminants (*1*). It has many advantages over other treatment methods, such as environmental friendliness, ability to be performed at ambient temperatures, and effectiveness to mineralize organic compounds even at low concentrations (*1, 2*). TiO_2 has proven to be one of the most excellent photocatalysts for the oxidative decomposition of many organic compounds, but it can only be excited by UV or near-UV radiation due to its wide band gap of 3.2 eV, hindering practical applications (*1*). To efficiently utilize visible light (VL) that covers the largest proportion of the solar spectrum, the development of visible-light-driven (VLD) photocatalysts has attracted a tremendous amount of attention.

Recently, $In(OH)_3$, a wide band gap semiconductor (Eg = 5.17 eV), has been shown to exhibit superior photocatalytic activity in the photodegradation of benzene when compared with TiO_2 under 254 nm UV irradiation (*3*). Since its wide band gap is related to the deep potential of O 2p orbitals, Li et al. (*3*) succeeded in narrowing the band gap of $In(OH)_3$ by partial substitution of OH^- by S^{2-} to form In(OH)$_y$S$_z$ solid solution (In(OH)$_y$S$_z$-SS) due to a higher energy level of S 3p compared with that of O 2p. To achieve a more suitable band structure for VLD photocatalysis, Fu's and Li's groups (*4, 5*) have prepared Zn: In(OH)$_y$S$_z$-SS and Cu:In(OH)$_y$S$_z$-SS by doping Zn^{2+} or Cu^{2+} cation in In(OH)$_y$S$_z$-SS in an aqueous solution of ethylenediamine. However, there is a lack of systematic study of the photocatalytic reactions, and the details of the reaction mechanism(s) are still unclear. The most interesting questions are (1) what kinds of reactive species are mainly generated during the photocatalytic process for the degradation of pollutants? and (2) is the direct contact between the catalysts and pollutants a prerequisite for the efficient degradation of pollutants?

It is well-known that the photocatalytic activity is closely related to the size, morphology, and structure of the photocatalysts (*6*–*8*). Semiconductors with two-dimensional (2D) nanostructure such as nanoplates have attracted increasing attention in the photocatalytic field because of their high crystallinity and extremely high anisotropy with ultrathin thickness (*9*). In the present work, we report the synthesis of Zn:In(OH)$_y$S$_z$-SSN using a hydrothermal reaction assisted by sodium dodecyl sulfate (SDS) instead of ethylenediamine. The effects of SDS, $Zn(NO_3)_2$ or thiourea concentration on the phase, photoabsorption, and morphology of solid solutions and their photocatalytic activities were investigated. In particular, we have developed a simple and versatile strategy to confirm the fact that direct contact between the Zn:In(OH)$_y$S$_z$-SSNs and pollutants is a prerequisite for the photocatalytic degradation of pollutants.

2. Experimental Section

2.1. Preparation of Photocatalysts. The photocatalysts were prepared by hydrothermal synthesis methods. All of the reagents were analytical grade and used without further purification. $In(OH)_3$ was prepared with 1.5 mmol $In(NO_3)_3 \cdot 5H_2O$ as the only precursor in a 50-mL Teflon-lined stainless steel autoclave. For the preparation of In(OH)$_y$S$_z$ and Zn:In(OH)$_y$S$_z$, desired amounts of thiourea (0−3 mmol),

* Corresponding author tel: +852-2609 6383; fax: +852-2603 5767; e-mail: pkwong@cuhk.edu.hk.
[†] Department of Biology, The Chinese University of Hong Kong.
[‡] Department of Chemistry, The Chinese University of Hong Kong.
[§] State Key Laboratory of Environmental Aquatic Chemistry, Research Center for Eco-Environmental Sciences, Chinese Academy of Sciences.
[∥] Department of Microbiology, The Chinese University of Hong Kong.
[⊥] Environmental Science Programme, The Chinese University of Hong Kong.

10.1021/es902013d CCC: $40.75
Published on Web 09/02/2009

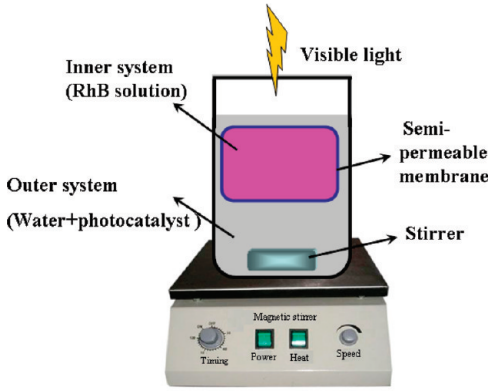

FIGURE 1. Schematic illustration of setup for the separation system.

SDS (0−80 mmol), and $Zn(NO_3)_2 \cdot 6H_2O$ (the atomic ratio of Zn^{2+} to In^{3+} in the synthesis solution, hereafter simplified as X) were added. Then, the pH value of all the precursor suspensions was adjusted to 11 using a 2 mol L^{-1} NaOH solution. Subsequently, the suspensions were autoclaved and maintained at 160 °C for 24 h. The precipitates were collected by centrifugation and washed three times with water, and then washed three times with ethanol. After drying at 80 °C, the products were obtained.

2.2. Characterization of Catalysts. Transmission electron microscope (TEM) analyses were performed with a FEI TECNAI F20 field emission electron microscope. X-ray diffraction (XRD) patterns were recorded on a Huber diffractometer (V612365) equipped with a rotating anode and using Cu Kα radiation (Rigaku, Ru-300). UV−visible absorption spectra of the samples were recorded on a UV−vis spectrophotometer (JASCO V-550, Japan) with an integrating sphere attachment. Nitrogen adsorption−desorption isotherms were collected at 77 K using Micromeritics ASAP2010 equipment (BET for specific surface area).

2.3. Photocatalytic Activity. The photocatalytic activities of the photocatalysts were evaluated by the degradation of RhB using a 300 W xenon lamp (Beijing Perfect Light Co. Ltd., Beijing) with a cutoff filter ($\lambda > 400$ nm) as light source. In each experiment, 10 mg of photocatalyst was added into 100 mL of 5 mg L^{-1} RhB aqueous solution. Before irradiation, the suspensions were magnetically stirred in dark for 60 min to ensure the establishment of an adsorption/desorption equilibrium between the photocatalyst and RhB. At given time intervals, 1.5 mL of suspension was sampled and centrifuged to remove the photocatalyst particles. The residual RhB in the solution was analyzed by recording variations at the wavelength of maximal absorption (553 nm) in the UV−vis spectra of RhB with a UV-3600 (Shimadzu, Japan) spectrophotometer.

To investigate whether the direct contact between Zn:$In(OH)_yS_z$-SSN and RhB is a prerequisite for photocatalytic degradation, a semipermeable membrane was used to separate the RhB and Zn:$In(OH)_yS_z$-SSNs. The setup of the separated system for this experiment is shown as Figure 1. The initial concentration of RhB in the solution (20 mL) contained in the membrane packaged container is 2.6 mg L^{-1}. The outer system contained 50 mL of the aqueous suspension including 10 mg of Zn:$In(OH)_yS_z$-SSNs, and the suspension was stirred continuously to keep the Zn:$In(OH)_yS_z$-SSNs evenly distributed in the solution outside of the container. The whole beaker was placed under the xenon lamp, allowing the light to focus onto the solution. After 1 h, 1.5 mL of solution both outside and inside of the container was sampled to detect the concentration of RhB. The outer system was also replaced by pure water, H_2O_2 solution, Fenton reagent without light irradiation, or TiO_2 suspension irradiated by UV light in a series of comparison experiments.

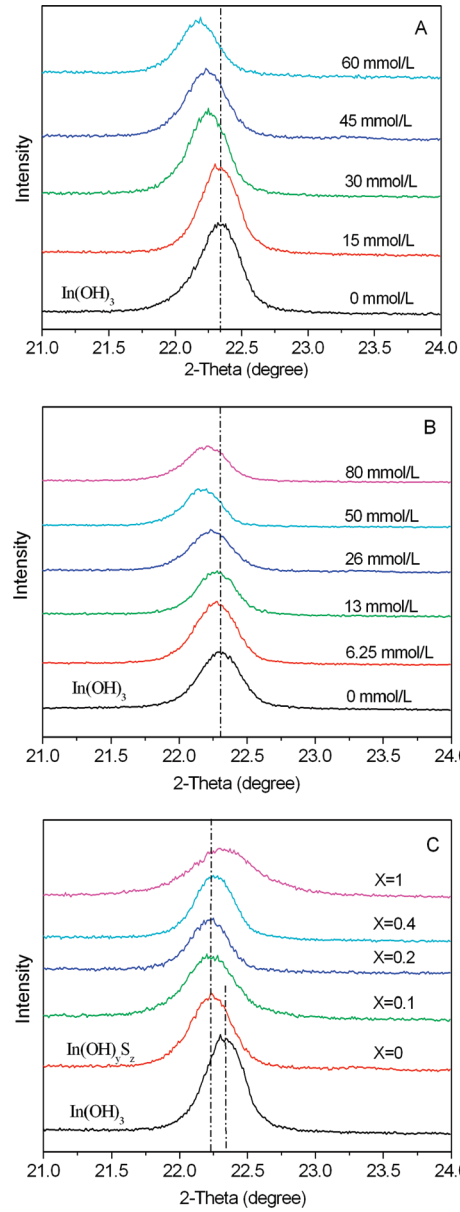

FIGURE 2. Enlarged XRD patterns of $In(OH)_3$, $In(OH)_yS_z$, and Zn:$In(OH)_yS_z$-SS synthesized under various conditions. A: $In(OH)_3$ and $In(OH)_yS_z$ synthesized with the concentration of thiourea varied from 15 to 60 mmol L^{-1} ([SDS] = 26 mmol L^{-1}, $X = 0$); B: $In(OH)_3$ and $In(OH)_yS_z$ synthesized with SDS concentrations varied from 6.25 to 80 mmol L^{-1} ([thiourea] = 45 mmol L^{-1}, $X = 0$); C: $In(OH)_3$, $In(OH)_yS_z$, and Zn:$In(OH)_yS_z$ synthesized with X value varying between 0.1 and 1 ([thiourea] = 45 mmol L^{-1}, [SDS] = 26 mmol L^{-1}). Samples were synthesized in aqueous solution at 160 °C for 24 h.

3. Results and Discussion

3.1. Preparation and Characterization of the Catalysts. The phases of $In(OH)_3$, $In(OH)_yS_z$, and Zn:$In(OH)_yS_z$-SS samples were examined by XRD. All $In(OH)_yS_z$ and Zn:$In(OH)_yS_z$-SS exhibit single-phase diffraction patterns, indicative of the cubic structure similar to $In(OH)_3$ (Figure S1). To facilitate the analysis, enlargements of the XRD patterns from 21 to 24° for these samples are depicted in Figure 2. The samples prepared in the absence of thiourea or SDS exhibit diffraction peaks indexed to pure cubic $In(OH)_3$ with calculated lattice constant $a = 7.959$ Å, in agreement with reported values

(JCPDS 85−1338; $a = 7.979$ Å). With the increase of thiourea concentration from 0 to 60 mmol L^{-1} or an increase of SDS concentration from 0 to 80 mmol L^{-1} in the synthesis solution, the diffraction peaks slightly shifts to low angles (Figure 2A and B), revealing that S^{2-} is homogeneously incorporated into the lattice of $In(OH)_3$ to form an $In(OH)_ySz$-SS. Considering the difference between the ionic radius of S^{2-} (1.84 Å) and the thermochemical radius of OH^- (1.40 Å), the low angle shift of the diffraction peaks is reasonable (*3*). When thiourea concentration is higher than 60 mmol L^{-1} or SDS concentration is up to 100 mmol L^{-1}, the diffraction peaks do not shift further, while a diffraction peak corresponding to β-In_2S_3 begins to appear. Moreover, increasing SDS concentrations result in lower diffraction intensities of samples (Figures 2B and S1B), indicating a decrease in crystallization. Zn:$In(OH)_ySz$-SS was realized by adding Zn^{2+} cations into the synthesis solution. Clearly, with the increase of X value from 0 to 1, the peak of Zn:$In(OH)_ySz$ shifts to a slightly larger angle (Figure 2C), suggesting that Zn^{2+} is homogeneously located in the lattice of $In(OH)_ySz$. It is also speculated that Zn^{2+} is substituted for In^{3+} in the lattice of $In(OH)_ySz$ due to the slightly larger ionic radius of In^{3+} (0.81 Å) than that of Zn^{2+} (0.74 Å) (*4*). Furthermore, the existence of Zn element as Zn^{2+} and S element as S^{2-} in the Zn:$In(OH)_ySz$-SS was confirmed by the high-resolution XPS spectra of the Zn 2p3/2 and S 2p3/2 region (Figure S2), which again supports the formation of Zn:$In(OH)_ySz$-SS.

Figure 3 shows the UV−vis diffuse reflectance spectra (DRS) of $In(OH)_3$, $In(OH)_ySz$, ZnS, and Zn:$In(OH)_ySz$-SS samples. As shown in Figure 3A and B, the pure $In(OH)_3$ sample obtained in the absence of thiourea or SDS has an adsorption edge at 240 nm and a band gap of 5.17 eV, which is consistent with that reported by Avivi et al. (*10*). With increasing thiourea or SDS concentration in the synthesis solution, not only does the adsorption for $In(OH)_ySz$ increase in intensity, but also its absorption edge red-shifts (Figure 3A and B). The band gap, estimated from the onset of the absorption edge for $In(OH)_ySz$-SS, decreases from 5.17 to 2.09 eV when the thiourea concentration increases from 0 to 60 mmol L^{-1}, and from 5.17 to 2.01 eV when the SDS concentration increases from 0 to 50 mmol L^{-1}. Theoretical calculations indicate that the valence band (VB) of indium oxide is dominated by O 2p, whose potential is much more positive than that of S 3p (*3*). Thus, the more S^{2-} is substituted for OH^- in $In(OH)_3$, the less positive the new VB and the smaller the band gap of $In(OH)_ySz$-SS formed by the hybridization of O 2p and S 3p are. For the Zn:$In(OH)_ySz$-SSs, their absorption edge is located between those of ZnS and $In(OH)_ySz$, and shifts monotonously from 560 to 405 nm with an increase of X from 0 to 1, corresponding to an increase in the band gap from 2.21 to 3.06 eV, as shown in Figure 3C. No absorption ascribed to ZnS was observed, confirming that the Zn^{2+} is homogeneously doped into the lattice of $In(OH)_ySz$. Moreover, Zn:$In(OH)_ySz$-SSs with low Zn doping exhibits steep edges and strong absorption in the VL region, suggesting that the absorption is due to direct transitions between the VB and the conduction band (CB) of the Zn:$In(OH)_ySz$-SS .

SDS not only plays an important role in the substitution of S^{2-} to form Zn:$In(OH)_ySz$-SS, but also significantly influences their morphologies. Typical morphologies of the Zn:$In(OH)_ySz$-SSs synthesized with different SDS concentrations in the synthesis solution were characterized by TEM and HRTEM, as shown in Figure 4. Zn:$In(OH)_ySz$-SS exhibits a rectangular-plate shape, with an average width of about 10 nm and an average length of about 15 nm when the SDS concentration is 26 mmol L^{-1} (Figure 4A). The HRTEM image (inset of Figure 4A) further demonstrates the clear lattice fringes with lattice spacing of 0.42 nm, which is slightly larger than the value of the (200) plane of the cubic $In(OH)_3$ ($d =$ 0.40 nm), mainly due to larger ionic radius of S^{2-} (1.84 Å) compared to the thermochemical radius of OH^- (1.40 Å) (*3*, *4*). With increasing concentrations of the SDS surfactant, the

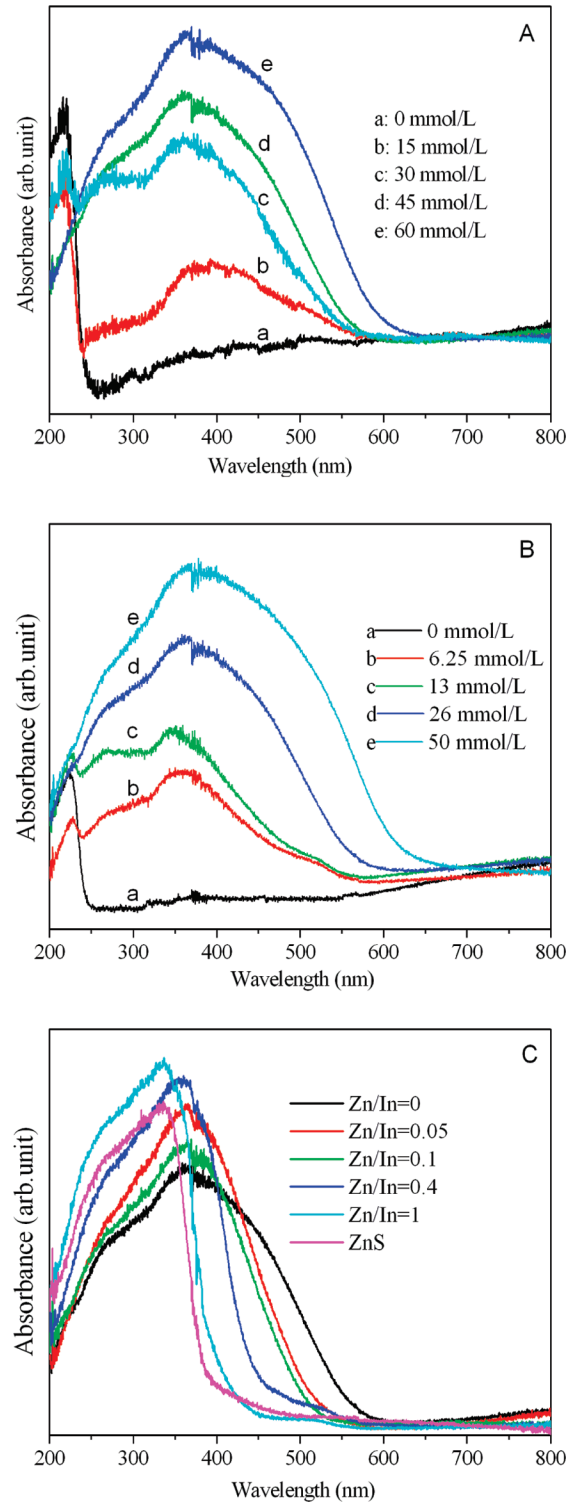

FIGURE 3. UV−vis DRS of In $(OH)_3$, In$(OH)_ySz$, ZnS, and Zn:In$(OH)_ySz$ samples synthesized under various conditions. A: In$(OH)_3$ and In$(OH)_ySz$ synthesized with thiourea concentrations varying from 15 to 60 mmol L^{-1} ([SDS] = 26 mmol L^{-1}, X = 0); B: In$(OH)_3$ and In$(OH)_ySz$ synthesized with SDS concentrations varied from 6.25 to 50 mmol L^{-1} [thiourea] = 45 mmol L^{-1}, X = 0); C: ZnS, In$(OH)_3$, In$(OH)_ySz$, and Zn:In$(OH)_ySz$ synthesized with X value varying from 0.05 to 1 ([thiourea] = 45 mmol L^{-1}, [SDS] = 26 mmol L^{-1}). Samples were synthesized in aqueous solution at 160 °C for 24 h.

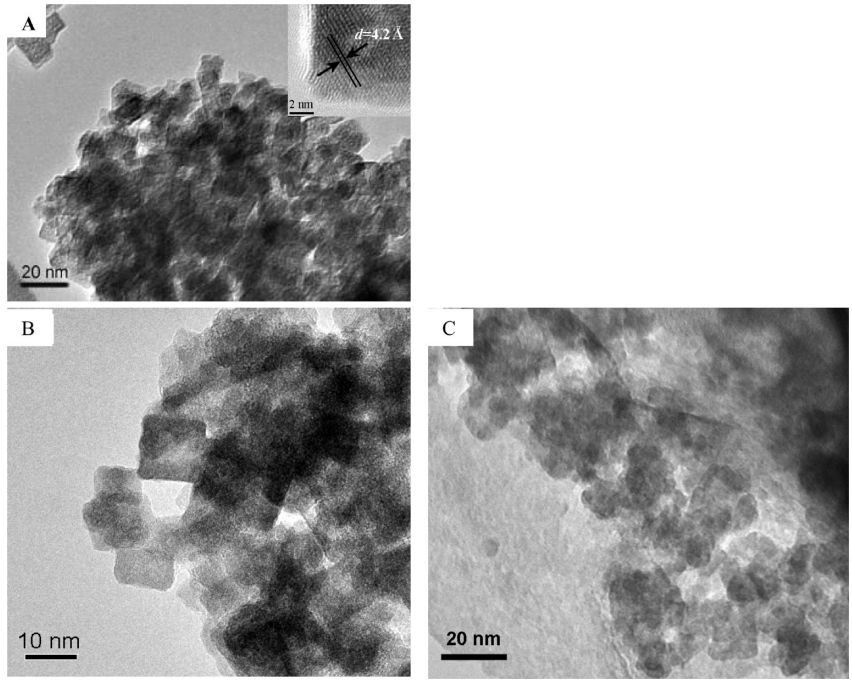

FIGURE 4. TEM and HRTEM images of Zn:In(OH)$_y$S$_z$-SS ([thiourea] = 45 mmol L^{-1}, X = 0.3) with different SDS concentration: A, 26 mmol L^{-1}; B, 50 mmol L^{-1}; C, 80 mmol L^{-1}.

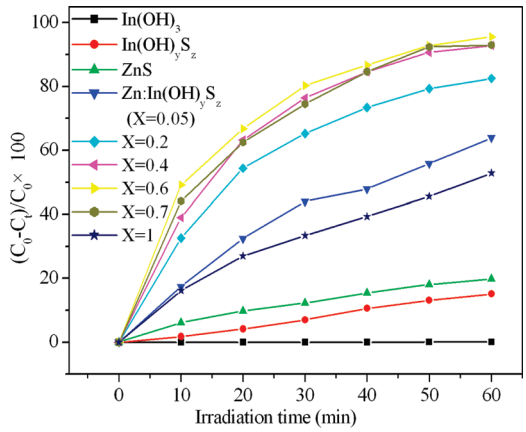

FIGURE 5. Photodegradation efficiencies of RhB (5 mg L^{-1}, 100 mL) by different photocatalysts (100 mg L^{-1}) as a function of irradiation time under visible light.

rectangular nanoplate tends to be transformed into smaller square nanoplates, meanwhile part of the nanoplates display truncated corners or some breakage of the edges, resulting in irregular outlines (Figure 4B). Eventually, when the concentration of SDS was further increased to 80 mmol L^{-1}, only spherical particles with an average diameter about 8 nm could be observed, instead of a plate-like morphology (Figure 4C).

3.2. Photocatalytic Properties. *3.2.1 Photocatalytic Performance.* RhB, a widely used dye, was chosen as a representative pollutant to evaluate the photocatalytic performance of the photocatalysts. Figure 5 shows the photocatalytic performances of different photocatalysts by comparing the degradation efficiency of RhB with otherwise identical conditions under VL. ZnS, a UV-excited photocatalyst, shows some photoactivity and degrades 19.8% of RhB within 60 min because ZnS can easily be photosensitized by dyes (*11*). In contrast, In(OH)$_3$, with a wide band gap of 5.17 eV, has no photoactivity under VL, indicating that the photoexcited electron of RhB cannot efficiently transfer to the CB of In(OH)$_3$. When OH$^-$ in In(OH)$_3$ is partly substituted by S^{2-}, a VL response of In(OH)$_y$S$_z$-SS is induced by the excitations from the new VB formed by the hybridization of O 2p with S 3p to the CB (*3*, *4*). Thus, the VLD photocatalytic efficiency enhanced from 0% to 15%. However, this degradation efficiency is inadequate to meet modern environmental remediation goals. It is well-known that the position of the CB is also a crucial factor influencing the photoactivity of semiconductors. Only the photogenerated holes in the VB of In(OH)$_y$S$_z$ can be utilized to degrade the organic pollutants (*3*). To obtain a high charge-utilization rate, the level of the CB should be much more negative so that the photogenerated electrons have enough power to reduce the surface chemisorbed O$_2$, generating superoxide radical (*12*). Fortunately, the energy level of Zn 4s4p is more negative than that of In 5s5p (*4*). With the Zn^{2+} incorporation, the new CB in the Zn:In(OH)$_y$S$_z$-SS introduced by the hybridization of the In 5s5p with Zn 4s4p will shift to a more negative energy level. This more negative energy level of the CB facilitates the reduction of surface-adsorbed oxygen to form more reactive species such as $\cdot O_2^-$ and $\cdot$OH to degrade the organic pollutant (*12*). This scavenging of CB electrons is crucial to prevent charge recombination and loss of reaction efficiency (*13*). Therefore, the photocatalytic activity of Zn:In(OH)$_y$S$_z$-SS is enhanced with an increase in the incorporation of Zn^{2+} (Figure 5). Remarkably, the maximum photocatalytic efficiency reaches 95.6% after 60 min when the X value is 0.6, but the photocatalytic efficiency decreases with a higher ratio of Zn/In (X ≥ 0.7) due to less photoabsorption in the VL range, which is reflected in the UV−vis DRS (Figure 3C).

The morphology and crystallinity also greatly influence the photocatalytic performance. Figure 6 shows the photodegradation efficiencies of RhB by Zn:In(OH)$_y$S$_z$-SS with various SDS concentrations under VL. Zn:In(OH)$_y$S$_z$-SS with a nanoplate structure prepared in the presence of 26 mmol L^{-1} SDS (Figure 4A) has a higher photocatalytic activity than that prepared with 50 or 80 mmol L^{-1} SDS (Figure 4B and C). There are two possible explanations for these results: the first is that the high anisotropy, with an ultrathin nanoplate structure, allows the photogenerated holes and electrons inside the crystalline to transfer more easily to the surface, which facilitates the participation of photogenerated charges in photocatalytic reactions (*9*); the second should be at-

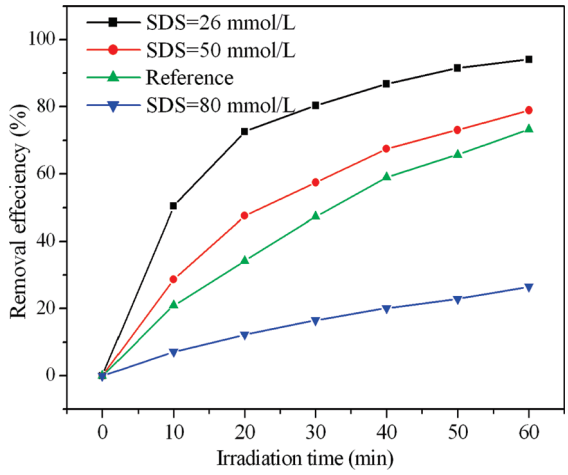

FIGURE 6. Photodegradation efficiencies of RhB (5 mg L^{-1}, 100 mL) by 10 mg Zn:In(OH)$_y$S$_z$-SS prepared at different SDS concentration as well as Zn:In(OH)$_y$S$_z$-SS prepared in aqueous solution of ethylenediamine (*4*) under visible light irradiation.

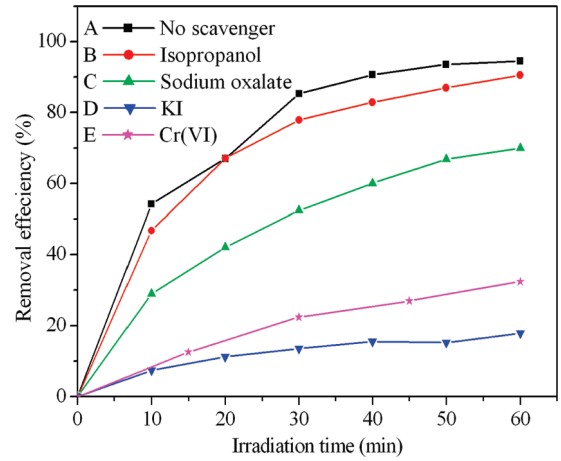

FIGURE 7. Photodegradation efficiencies of RhB (5 mg L^{-1}, 100 mL) by 10 mg of Zn:In(OH)$_y$S$_z$-SSN (X = 0.5) with scavenger (10 mmol L^{-1} isopropanol, sodium oxalate, KI, and 0.5 mmol L^{-1} Cr(VI)) under visible light irradiation.

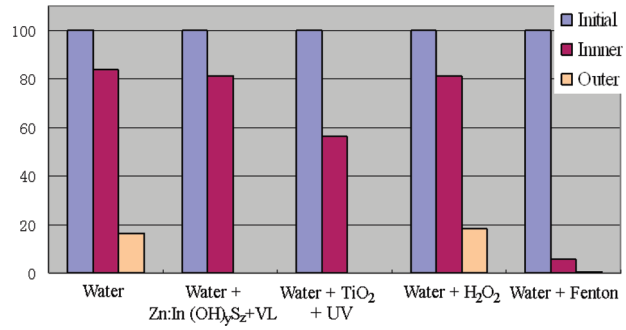

FIGURE 8. Percentages of RhB inside and outside a semipermeable membrane packaged container when the outer system is in various conditions. The initial concentration of RhB is 2.6 mg L^{-1}. A, water; B, water + Zn:In(OH)$_y$S$_z$ + VL; C, water + TiO_2 + UV; D, water + H_2O_2; E, water + Fenton reagent.

tributed to the degree of crystallinity of the samples (*8*). The high photocatalytic activity of the Zn:In(OH)$_y$S$_z$-SSN probably also derives from its higher crystallinity (Figures 2B and S1B). Compared with the Zn:In(OH)$_y$S$_z$-SS (BET surface area of 91.8 m^2 g^{-1}) synthesized in an aqueous solution of ethylenediamine (*4*) (Figure S3), the Zn:In(OH)$_y$S$_z$-SSN prepared using SDS (Figure 4A) exhibits a much higher photocatalytic activity, as demonstrated in Figure 6. It is reasonable because the Zn:In(OH)$_y$S$_z$-SSN prepared using SDS have smaller and uniform particle size, and larger BET surface area of 233.5 m^2 g^{-1}. The smaller particle size can reduce the recombination of photogenerated charge carriers (*7*), and the larger BET surface area benefits the adsorption of pollutants and can supply more active reaction sites for the degradation of a pollutant (*6, 14*).

The photochemical experiments were also extended to another colorless organic, pentachlorophenol (PCP), that only has light absorption in the UV region. The PCP was degraded by Zn:In(OH)$_y$S$_z$-SSN upon VL irradiation in a fashion similar to that of the degradation of RhB but a longer irradiation time was required (Figure S4). Hence, Zn:In(OH)$_y$S$_z$-SSN is indeed a VL induced photocatalyst.

3.2.2. Photocatalytic Mechanism(S). As mentioned above, the holes, $\cdot O_2^-$ and ·OH are considered to be major reactive species for the photocatalytic degradation of RhB. Several scavengers were employed to further confirm the specific reactive species that play important roles in this VLD photocatalytic process: sodium oxalate for holes (*15*), KI for holes and $\cdot OH_s$ on photocatalyst (*16*), isopropanol for ·OH in the bulk (*16, 17*) (denoted as $\cdot OH_b$), and Cr(VI) for electrons (*16*). Figure 7 shows the photodegradation efficiencies of RhB by Zn:In(OH)$_y$S$_z$-SSN in the presence of these scavengers under VL. Isopropanol is easily oxidized by ·OH radicals and so it is usually used as a diagnostic tool for $\cdot OH_b$ due to its low affinity to semiconductor surfaces in aqueous media (*16, 17*). Notably, as can be seen in Figure 7B, the addition of isopropanol has little influence on the photodegradation of RhB, indicating that there is little $\cdot OH_b$. However, in the presence of sodium oxalate, the photodegradation of RhB declines to 69% after 60 min irradiation. With the addition of KI, the decolorization rate of RhB drops sharply and only 17% of RhB is degraded after 60 min. Upon purging with nitrogen and the addition of Cr(VI), the role of species generated at the reduction site on the surface of photocatalyst such as $\cdot O_2^-$ and $\cdot OH_s$ could be ignored, since the photogenerated electrons are quenched by Cr(VI) (*16*). Thus, in the presence of 0.5 mmol L^{-1} $K_2Cr_2O_7$ upon purging with nitrogen, the photodegradation efficiency reaches only 32%. Therefore, it is concluded that the holes, $\cdot O_2^-$ and $\cdot OH_s$ existing on the surface of Zn:In(OH)$_y$S$_z$-SSN are the major reactive species responsible for the photocatalytic degradation of RhB. Therefore, the photocatalytic degradation of RhB only occurs on the surface of the Zn:In(OH)$_y$S$_z$-SSN. As expected, the more adsorption of RhB by Zn:In(OH)$_y$S$_z$-SSN, the higher photocatalytic degradation efficiency of RhB results (Figure S5).

However, whether direct contact of the Zn:In(OH)$_y$S$_z$-SSN with RhB is necessary for photocatalytic degradation of RhB remains a question. To clarify this question, we have constructed a novel and simple setup in which a semipermeable membrane is used to allow the free entry of ions and radicals such as ·OH and $\cdot O_2^-$ but only slow leakage of RhB, as shown in Figure 1. Figure 8 shows the percentages of RhB in or out of the semipermeable membrane-packaged container for different outer systems. When the outer system contains only water, 83.5% of the RhB is kept within the membrane packaged-container and 16.5% of the RhB diffuses into the outer water after 1 h. However, when the outer system is a Fenton reagent, only 5% of the RhB remains in the container and no RhB is detected outside after 1 h, because ·OH generated by the Fenton reagent can pass through the membrane and degrade RhB both inside and outside the container. It also can be seen that only H_2O_2 is unable to degrade the RhB within 1 h. When employing water, TiO_2, and UV light as the outer system, the percentage of RhB in the container declines to 56% after 1 h, which mainly results from the diffusion of reactive oxygen species such as ·OH

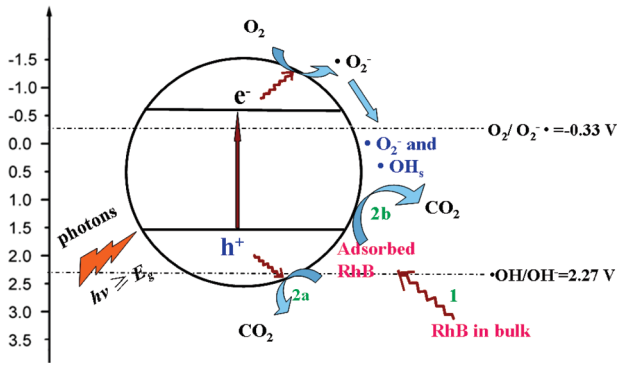

FIGURE 9. Schematic illustration of the process of photocatalytic degradation of RhB by the Zn:In(OH)$_y$S$_z$-SSN under visible light.

generated in the TiO_2-mediated photocatalytic process (*18, 19*). However, with water, Zn:In(OH)$_y$S$_z$-SSN, and VL as the outer system, the percentage of RhB in container shows no appreciable difference with that employing pure water as outer system, indicating that there is little entry of bulky ·OH or $\cdot O_2^-$ through the membrane. In contrast, the concentration of RhB in the outer solution is zero, which is similar to that in the TiO_2-mediated photocatalytic process, indicating that the leaked RhB is first adsorbed onto the surface of Zn:In(OH)$_y$S$_z$-SSN and then is photocatalytically degraded. These facts directly prove that direct contact between the Zn:In(OH)$_y$S$_z$-SS and RhB is the prerequisite for the photocatalytic degradation of RhB.

Based on the results above, the process of photocatalytic degradation of RhB by the Zn:In(OH)$_y$S$_z$-SS under VL is proposed as in Figure 9. With VL irradiation, electrons are promoted from the VB into the CB of Zn:In(OH)$_y$S$_z$-SS, leaving holes. Although these photogenerated holes cannot oxidize OH^- or H_2O into ·OH, they can oxidize organic pollutants adsorbed onto the surface of the catalyst (*3*), as shown in Step 2a in Figure 9. On the other hand, the photogenerated electrons in the CB have strong reductive ability and they can reduce the adsorbed oxygen into $\cdot O_2^-$. Then, part of the $\cdot O_2^-$ is further transformed into $\cdot OH_s$. These $\cdot OH_s$ and $\cdot O_2^-$ on the surface of Zn:In(OH)$_y$S$_z$-SS also can degrade the adsorbed RhB, as indicated in Step 2b in Figure 9. The location of these reactive species determines that photocatalytic degradation of RhB only occurs on the surface of Zn:In(OH)$_y$S$_z$-SS, which also explains why the morphology and BET area have a great influence on their photocatalytic activity, as discussed previously. Because there are few reactive species in the bulk solution, RhB in the bulk solution cannot be degraded spontaneously. Only after the adsorbed RhB is degraded, can more RhB in the bulk solution be adsorbed onto the surface of Zn:In(OH)$_y$S$_z$-SS (Step 1 in Figure 9) and further be degraded. In time, the RhB in suspension will be degraded to form smaller organic molecules, and these organic molecules can eventually be mineralized into CO_2 and H_2O, as revealed by GC-MS identification (Figure S7), and analyses of total organic carbon as well as evolved CO_2 and inorganic carbon (Figure S8).

Acknowledgments

The project was supported by a research grant (CUHK4585/06M) from the Research Grant Council, Hong Kong SAR Government, to P.K.W., C.H., J.C.Y., and C.Y.C.

Supporting Information Available

Additional details in 8 figures. This material is available free of charge via the Internet at http://pubs.acs.org.

Literature Cited

(1) Tang, J.; Zou, Z. G.; Ye, J. H. Efficient photocatalytic decomposition of organic contaminants over $CaBi_2O_4$ under visible-light irradiation. *Angew. Chem., Int. Ed.* **2004**, *43*, 4463–4466.
(2) Hoffmann, M. R.; Martin, S. T.; Choi, W.; Bahneman, D. W. Environmental applications of semiconductor photocatalysis. *Chem. Rev.* **1995**, *95*, 69–96.
(3) Li, Z. H.; Dong, T. T.; Zhang, Y. F.; Wu, L.; Wang, J. Q.; Wang, X. X.; Fu, X. Z. Studies on In(OH)$_y$S$_z$ solid solutions: Syntheses, characterizations, electronic structure, and visible-light-driven photocatalytic activities. *J. Phys. Chem. C* **2007**, *111*, 4727–4733.
(4) Lei, Z. B.; Ma, G.; Liu, M.; You, W.; Yan, H.; Wu, G.; Takata, T.; Hara, M.; Domen, K.; Li, C. Sulfur-substituted and zinc-doped $In(OH)_3$: A new class of catalyst for photocatalytic H_2 production from water under visible light illumination. *J. Catal.* **2006**, *237*, 322–329.
(5) Li, Z. H.; Dong, H.; Zhang, Y. F.; Dong, T. T.; Wang, X. X.; Li, J. Q.; Fu, X. Z. Effect of M^{2+} (M = Zn and Cu) dopants on the electronic structure and photocatalytic activity of In(OH)$_y$S$_z$ solid solution. *J. Phys. Chem. C* **2008**, *112*, 16046–16051.
(6) Kamat, P. V. Photochemistry on nonreactive and reactive (semiconductor) surfaces. *Chem. Rev.* **1993**, *93*, 207–300.
(7) Zhang, L. S.; Li, J. L.; Chen, Z. G.; Tang, Y. W.; Yu, Y. Preparation of Fenton reagent with H_2O_2 generated by solar light-illuminated nano-Cu_2O/MWNTs composites. *Appl. Catal. A* **2006**, *299*, 292–297.
(8) Zhang, L. S.; Wang, W. Z.; Chen, Z. G.; Zhou, L.; Xu, H. L.; Zhu, W. Fabrication of flower-like Bi_2WO_6 superstructures as high performance visible-light driven photocatalysts. *J. Mater. Chem.* **2007**, *17*, 2526–2532.
(9) Zhang, C.; Zhu, Y. Synthesis of square Bi_2WO_6 nanoplates as high-activity visible-light-driven photocatalysts. *Chem. Mater.* **2005**, *17*, 3537–3545.
(10) Avivi, S.; Mastai, Y.; Gedanken, A. Sonohydrolysis of In^{3+} ions: formation of needlelike particles of indium hydroxide. *Chem. Mater.* **2000**, *12*, 1229–1233.
(11) Zang, L.; Liu, C. Y.; Ren, X. M. Photochemistry of semiconductor particles 3. Effects of surface charge on reduction rate of methyl orange photosensitized by ZnS sols. *J. Photochem. Photobiol. A* **1995**, *85*, 239–245.
(12) Kormann, C.; Bahnemann, D. W.; Hoffmann, M. R. Photolysis of chloroform and other organic molecules in aqueous TiO_2 suspensions. *Environ. Sci. Technol.* **1991**, *25*, 494–500.
(13) Schmelling, D. C.; Gray, K. A.; Kamat, P. V. Role of reduction in the photocatalytic degradation of TNT. *Environ. Sci. Technol.* **1996**, *30*, 2547–2555.
(14) Wang, X. C.; Yu, J. C.; Ho, C. M.; Hou, Y. D.; Fu, X. Z. Photocatalytic activity of a hierarchically macro/mesoporous titania. *Langmuir* **2005**, *21*, 2552–2559.
(15) Jin, R. C.; Gao, W. L.; Chen, J. X.; Zeng, H. S.; Zhang, F. X.; Liu, Z. G.; Guan, N. J. Photocatalytic reduction of nitrate ion in drinking water by using metal-loaded $MgTiO_3$-TiO_2 composite semiconductor catalyst. *J. Photochem. Photobiol. A* **2004**, *162*, 585–590.
(16) Chen, Y. X.; Yang, S. Y.; Wang, K.; Lou, L. P. Role of primary active species and TiO_2 surface characteristic in UV-illuminated photodegradation of Acid Orange 7. *J. Photochem. Photobiol. A* **2005**, *172*, 47–54.
(17) Khodja, A. A.; Boulkamh, A.; Richard, C. Phototransformation of metobromuron in the presence of TiO_2. *Appl. Catal. B* **2005**, *59*, 147–154.
(18) Choi, W.; Kim, S.; Cho, S.; Yoo, H.; Kim, M. H. Photocatalytic reactivity and diffusing •OH radicals in the reaction medium containing TiO_2 particles. *Korean J. Chem. Eng.* **2001**, *18*, 898–902.
(19) Ishikawa, Y.; Matsumoto, Y.; Nishida, Y.; Taniguchi, S.; Watanabe, J. Surface treatment of silicon carbide using TiO_2(IV) photocatalyst. *J. Am. Chem. Soc.* **2003**, *125*, 6558–6562.

ES902013D